Luminescence properties of the solvothermally synthesized blue light emitting Mn doped Cu_2O nanoparticles

Kajari Das,[1] Shailesh N. Sharma,[2] Mahesh Kumar,[2] and S. K. De[1,a)]
[1]*Department of Materials Science, Indian Association for the Cultivation of Science, Jadavpur, Kolkata 700 032, India*
[2]*National Physical Laboratory, Dr. KS Krishnan Marg, New Delhi 110 012, India*

(Received 13 August 2009; accepted 29 December 2009; published online 29 January 2010)

The Cu_2O nanoparticles having average crystallite diameters ~8–16 nm were synthesized by a simple solvothermal method. The Mn was doped in the Cu_2O sample of crystallite size ~8 nm. The effects of the size and doping concentration on the crystal structures of the nanoparticles were investigated. The x-ray photoelectron spectroscopy studies clearly showed that the Mn was incorporated into the Cu_2O lattice as Mn^{2+} due to the substitution of the Cu^{+} ions by Mn^{2+} ions. The quantum confinement effects were observed in the nanoparticles. The multiple emissions from the Cu_2O were quenched in the Mn doped nanoparticles and only blue light emitting Cu_2O nanoparticles were obtained due to the transition $^4T_2 \rightarrow {}^6A_1$ of Mn. The effects of the doping concentration and the particle size on the relaxations dynamics of the Cu_2O nanoparticles were mainly investigated using photoluminescence decay. © *2010 American Institute of Physics*. [doi:10.1063/1.3295910]

I. INTRODUCTION

Copper (I) oxide (Cu_2O) has the promising applications in solar energy conversion and catalysis.[1–5] It is a prospective candidate for low-cost photovoltaic applications due to its high optical absorption coefficient, lower band gap energy (2.17 eV), and for low cost, nontoxic, and large natural abundance of the base material copper. Further opportunities in catalysis could be realized through the stabilization of specific phases of copper oxide. Therefore, it is of fundamental interest to prepare phase pure copper oxide nanocrystals to examine their crystal structure and characterize their optical properties. An investigation and understanding of size effects in such a system is also of interest due to the possibility of tuning its optoelectronic properties. It is also an ideal compound using as a dilute magnetic semiconductor (DMS) with high T_c.[6] As well as being a candidate for the basis of a DMS, it has potential for use in *p-n* junctions and spin-light-emitting diodes (LEDs). Cu_2O has a cubic structure with $a = 4.269$ Å,[7] and its *p*-type conductivity arises from copper vacancies which introduce an acceptor level 0.4 eV above the valence band (VB).[8]

Bulk cuprous oxide (Cu_2O) has direct forbidden band-gap of 2.17 eV.[9] The lowest of the conduction band (CB) and the top of the VB have the same parity, so that electric dipole transition between them is forbidden.[10] Quantum size effects on the optical properties of this type of direct band gap semiconductors are phenomenologically different from that of indirect band gap semiconductors. Therefore the optical properties of Cu_2O are complex as well as interesting. Cu_2O has large excitonic binding energy of about 140 meV. The crystalline Cu_2O with nanoscale dimensions could be anticipated to have spatially confined excitons and thereby increase their concentration. The large excitonic binding energy offers the possibilities to observe excitonic features in the absorption and luminescence spectrum.[11,12] Such unique electronic structures of Cu_2O spur a growing amount of interest in its crystalline nanostructures. Cubic crystalline structure and the electronic properties of Cu_2O stimulated many researchers to study optical and electronic properties in different shapes and sizes.[13–15]

The study of semiconductor nanoparticles or quantum dots is a major field of research in condensed matter physics. Particularly interesting are the quantum size effects on the optical properties of the semiconductor nanoparticles.[16,17] Moreover the doping of the semiconductor nanoparticles with transition metal ions has been the subject of research in recent years to find out the potential applications in photonic field.[18,19] The engineering of band gap and influencing physical, chemical, and electronic properties of the semiconductors are possible by the use of the right dopants. Norman *et al.*[20] showed the tuning of the emission energy of Mn doped ZnSe nanoparticles. The band gap tuning of the Mn doped CdS quantum dots were observed by Kim.[18] Mn doped Cu_2O has been extensively studied by the many researchers as a DMS,[21,22] but no detail study on the tuning of the optical properties of the Mn doped Cu_2O was done previously.

Many attempts have been made to synthesis Mn doped Cu_2O with different techniques, such as solid state reaction of Cu_2O and Mn_2O_3, radio-frequency magnetron sputtering deposition, pulse laser deposition method, etc.[21–23] In our present work, Mn doped Cu_2O is prepared in the solution route. Solvothermal process is the most useful technique to synthesize undoped and doped nanocrystalline materials with different morphologies and sizes without using any template or matrix. Under solvothermal process, some properties of the solvents like density, viscosity, and diffusion coefficient

a)Author to whom correspondence should be addressed. Tel.: +91-33-2473-3073. FAX: +91-33-2473-2805. Electronic mail: msskd@mahendra.iacs.res.in.

TABLE I. Size of the nanocrystallites and the average microstrains calculated from Williamson–Hall formula and lattice parameter and *d*-spacing (d_{111}) calculated using POWD.

Sample name	Reaction parameters	Crystallites size from Williamson–Hall formula (nm)	Micro strain from Williamson–Hall formula (10^{-4})	Lattice parameter (a) and *d*-spacing (d_{111}) (Å)
CP1	180 °C, 2 h	16.36 ± 0.23	37.5 ± 1.39	a=4.2377 d_{111}=2.4466
CP2	160 °C, 2 h	11.56 ± 0.84	88.5 ± 11.7	a=4.2748 d_{111}=2.4681
CP3	140 °C, 2 h	8.35 ± 0.83	92.8 ± 13.7	a=4.2752 d_{111}=2.4683
LMnCP3 (0.3% Mn)	140 °C, 2 h	8.36 ± 1.25	100 ± 15	a=4.276 d_{111}=2.4687
MMnCP3 (1.5% Mn)	140 °C, 2 h	8.39 ± 0.95	102.7 ± 33.6	a=4.2783 d_{111}=2.4701
HMnCP3 (2.6% Mn)	140 °C, 2 h	8.46 ± 1.46	110.2 ± 54.9	a=4.2805 d_{111}=2.4714

change dramatically and the solvent behaves much differently from that expected at the normal conditions. Consequently, the solubility, diffusion process, and the chemical reactivity of the reactants are greatly enhanced.

In the present work, we have synthesized phase pure Cu_2O nanoparticles by a simple solvothermal method and studied the effects of the particle size and Mn doping on the optical properties of the Cu_2O nanoparticles. Excellent engineering of the luminescence properties has been done by the Mn doping. We have investigated the crystalline quality of the undoped and Mn doped nanoparticles using Williamson–Hall equation. From x-ray photoelectron spectroscopy (XPS) studies the valance states of the Cu and Mn have been found.

II. EXPERIMENT

All the chemical reagents used in this experiment were analytical grade and were used without further purification. In a typical procedure, 1.27 g of cupric acetate monohydrate ($CuAc_2$) was mixed with 48 ml ethanol (EtOH) under constant magnetic stirring for 1 h to prepare a homogeneous solution, then 0.0845 g of dextrose was added to the solution. After 1h constant magnetic stirring, the greenish solution gradually turned to the bluish green. The homogeneous solution was then transferred to a Teflon-lined stainless steel autoclave with 60 mL capacity and heat treated at different temperatures 140–180 °C for 2 h and the samples were denoted by CP3, CP2, and CP1 respectively (Table I). Likewise to study the effects of the Mn doping on the crystal quality and optical properties of the Cu_2O nanostructures, manganese acetate [$MnAc_2, 4H_2O$], was mixed in the above experimental solution and the solution was finally heat treated at 140 °C for 2 h. The products obtained were named as LMnCP3, MMnCP3, and HMnCP3 with different Mn concentrations of 1%, 3%, and 5% respectively (Table I). For all the above cases, the autoclave chambers were air cooled to room temperature after the reactions. The resulting precipitates were recovered by centrifugation and washed several times with distilled water, and the precipitates were finally vacuum dried for 4 h.

The crystalline phases of the products were determined by x-ray powder diffraction by using a Seifert 3000P diffractometer with Cu $K\alpha$ radiation (λ=1.54 Å). Microstructural properties were obtained using transmission electron microscope (TEM) (JEOL 2010). For the TEM observations, the powders were dispersed in 2-propanol and ultrasonicated for 15 min. A few drops of this ultrasonicated solution were taken on a carbon coated copper grid. Compositional analysis was performed by energy dispersive x-ray analysis (EDAX) (Kevex, Delta Class I) attached with the field-emission scanning electron microscope. To analyze the valance states of the constituents of the undoped and Mn doped Cu_2O, x-ray photoelectron spectroscopy (XPS) was recorded with a Perkin Elmer PHI 1257 spectrometer using a dual anode (Al/Mg) x-ray source. Optical absorbance of the samples was recorded via a UV-vis spectrophotometer (Shimadzu, UV-2450). The steady-state photoluminescence (PL) measurements were carried out at room temperature with a Fluorescence spectrometer (Hitachi, F-2500) using excitation wavelength 340 nm.

The luminescence decay curves were obtained by time correlated single-photon counting (TCSPC) (HORIBA JOBIN YVON IBH) via time-to-amplitude conversion. The samples were excited at the wavelength using LED (HORIBA JOBIN YVON IBH Nanoled–340) at a repetition rate of 1 MHz. The experimental time-resolved luminescence intensity decays I(t) have been analyzed by following multi-exponential model:

$$I(t) = b + \sum_{i=1}^{n} \alpha_i \exp(-t/\tau_i), \tag{1}$$

where n is the number of discrete emissive species, b is a baseline correction (dc offset), and α_i and τ_i are the pre-exponential factors and excited-state luminescence decay times associated with the ith component, respectively. $\Sigma\alpha_i$ is normalized to unity. The average decay time, $\langle\tau\rangle$ was calculated from

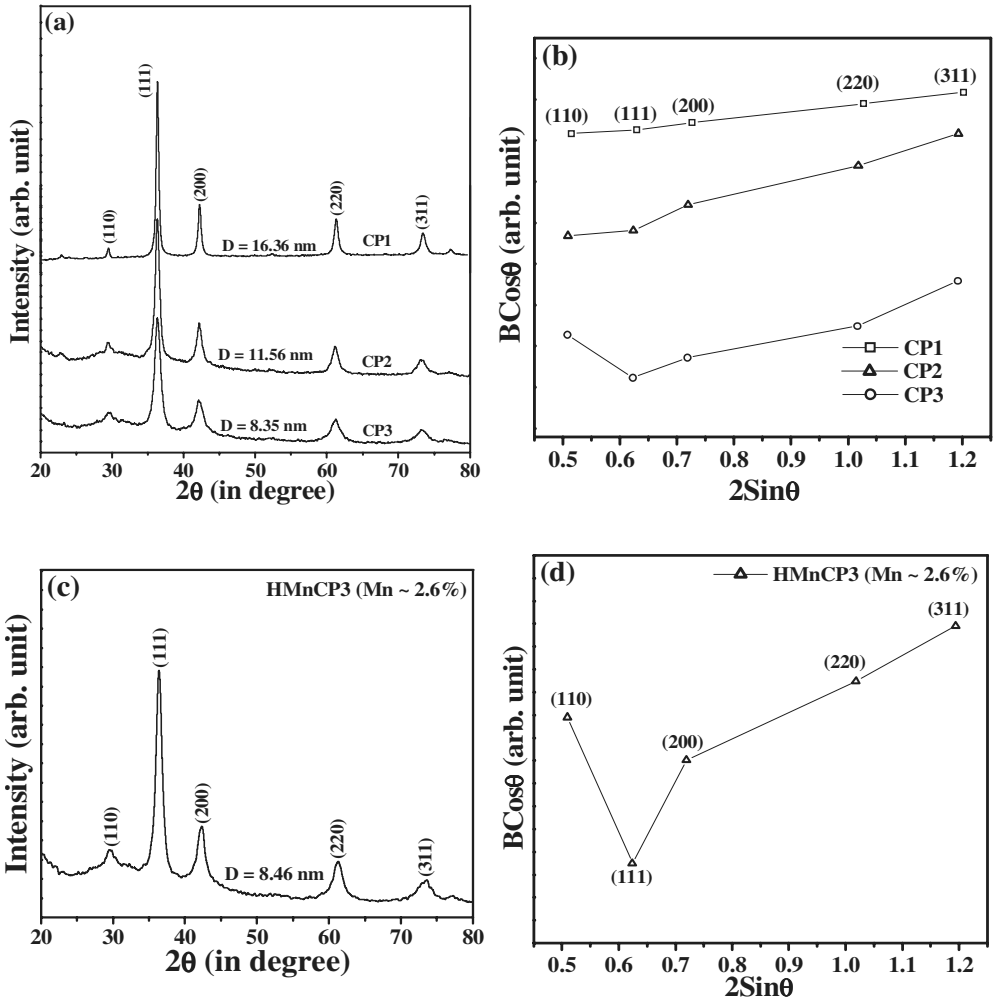

FIG. 1. (a) XRD spectra and (b) $B\cos\theta$ vs $2\sin\theta$ plots of the undoped samples CP1–CP3. (c) XRD spectrum and (d) $B\cos\theta$ vs $2\sin\theta$ plot of the 2.6% Mn doped sample HMnCP3.

$$\langle\tau\rangle = \frac{\sum_{i=1}^{n} \alpha_i \tau_i^2}{\sum_{i=1}^{n} \alpha_i \tau_i}. \quad (2)$$

The fractional contribution f_i of each decay component was estimated by the relation

$$f_i = \frac{\alpha_i \tau_i}{\sum_{j=1}^{n} \alpha_j \tau_j}, \quad (3)$$

where Σf_i is normalized to unity.

III. RESULTS AND DISCUSSIONS

X-ray diffraction (XRD) study was used to identify the phases and also estimate the sizes of the nanocrystallites. The XRD patterns of the three samples CP1–CP3 shown in Fig. 1(a) reveal that all the peaks correspond to the reflections from (110), (111), (200), (220), and (311) planes of cubic cuprous oxide (Cu_2O), which are consistent with the standard reported values.[24] Other impurities such as CuO and Cu are not found from the XRD spectra of the samples. The Williamson–Hall equation is used to calculate the crystallite size and microstrain for all the samples from XRD spectra.[25] The Williamson–Hall equation is expressed as follows:

$$B\cos\theta = \frac{0.89\lambda}{D} + 2(\varepsilon)\sin\theta, \quad (4)$$

where B is the full width at half maximum of the all XRD peaks, D is the crystallite size, λ the x-ray wavelength, θ the Bragg diffraction angle and ε the microstrain of lattice. In this method, $B\cos\theta$ is plotted against $2\sin\theta$ for all the samples shown in Fig. 1(b). Using a linear extrapolation to this plot, the intercept gives the crystallite size $0.89\lambda/D$ and the slope gives the micro strain ε. Here as the reaction temperatures were varied from 140–180 °C, the average sizes of the crystallites calculated were varied from 8.35 (±0.83)–16.36 (±0.23) nm shown in the Table I. It is clear from the literature that decreasing the crystallite size is associated with the increase in the dislocation densities, which introduces some micro strain in the lattice.[26] Average micro strain is also calculated from Williamson-Hall equation, shown in Table I, which indicates that the micro strain is maximum for the sample CP3 (crystallite size ~8.35 nm) and decreases with the increasing crystallite size. The values of the lattice parameter a and d-spacing (d_{111}) of the Cu_2O samples CP1–CP3 calculated using POWD (Ref. 27) are

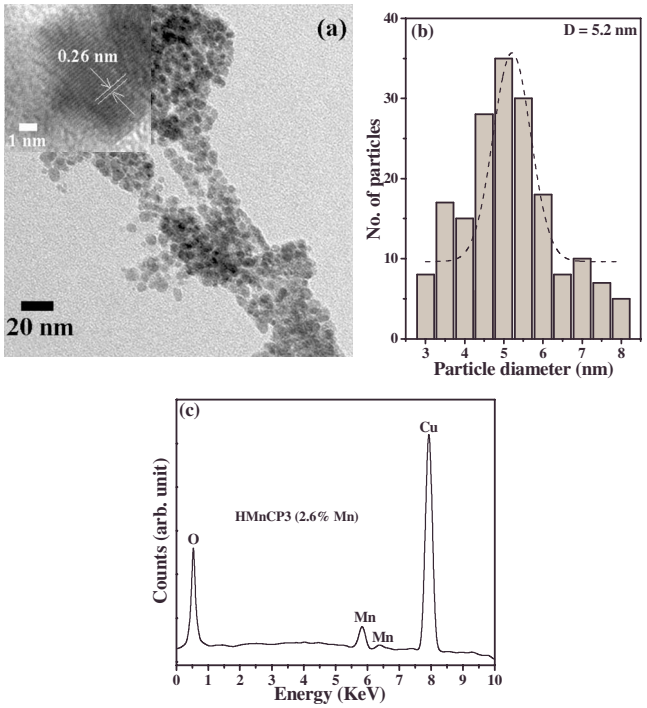

FIG. 2. (Color online) (a) Low resolution TEM image of the Cu_2O nanoparticles of sample CP3, inset shows the HRTEM image of a nanoparticle; (b) histogram plot for the particle diameter distribution corresponding to TEM image in (a), and (c) EDAX spectrum of the doped sample HMnCP3.

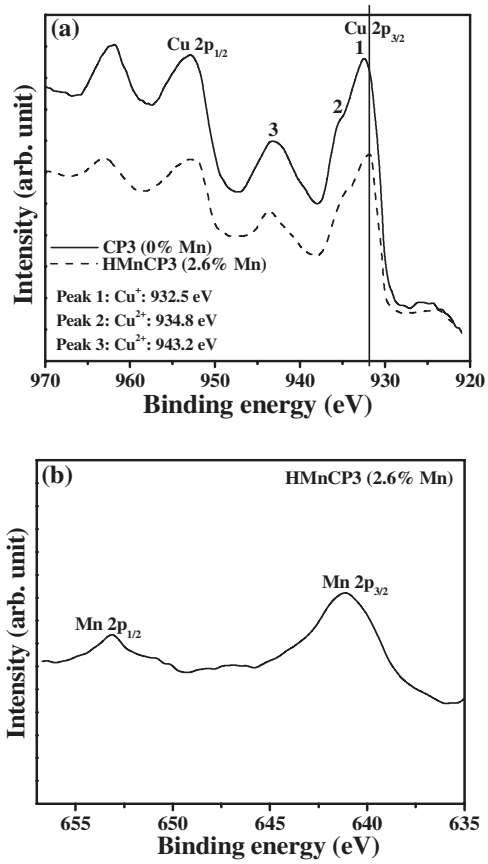

FIG. 3. XPS spectra of the (a) samples CP3 and HMnCP3 for Cu $2p$ peaks and (b) sample HMnCP3 for Mn $2p$ peak.

shown in Table I, indicate that the distortion of the lattice is more prominent in the smallest crystallite.

Mn doping in the sample CP3 (crystallite size 8.35 nm) produces more strain and lattice distortion in the crystal. The representative XRD pattern of the highest Mn doped sample HMnCP3 shown in Fig. 1(c) indicates the formation of pure phase Cu_2O without any impurities like CuO, Cu, and manganese oxide. The crystallite size and the microstrain were also calculated for all the doped samples LMnCP3–HMnCP3 using Williamson–Hall equation shown in the Table I. One representative plot of the Williamson–Hall equation, i.e., $B\cos\theta$ versus $2\sin\theta$ for the highest doped sample HMnCP3 is shown in Fig. 1(d). The lattice parameter a and d-spacing (d_{111}) values of all the doped samples were also calculated using POWD (Table I). From Table I, it is noted that the lattice parameter, d-spacing, and crystallite size were increased with increasing Mn concentration. The expansion of the lattice parameter and consequently the crystallite size of the doped samples with the Mn concentration may be explained by the substitutional incorporation of Mn into Cu sublattice, since Mn^{2+} for fourfold coordination with the high-spin state has a bigger effective ionic radius ~0.66 Å than that of Cu^+~0.46 Å for twofold coordination.[28]

The TEM image of the sample CP3 is shown in Fig. 2(a). The inset of the figure shows the HRTEM image of a nanoparticle, which indicates 0.26 nm spacing between two adjacent lattice planes of a nanoparticle corresponding to the (111) lattice planes of Cu_2O. Figure 2(b) represents the histogram plot for the particle diameter distribution corresponding to Fig. 2(a). The Gaussian fitting of the plot gives the average diameter of the nanoparticles ~5.2 nm.[29] For all other samples the average diameters of the nanoparticles were also calculated from the TEM images and histogram plots. The calculated diameters of the nanoparticles from the TEM images are well matched with the estimated sizes of the nanocrystallites from the XRD spectra.

The compositional analysis of the doped samples was carried out by EDAX. Figure 2(c) shows the one representative EDAX spectrum of the highest Mn doped sample HMnCP3. The concentrations of Mn in the samples LMnCP3, MMnCP3, and HMnCP3 found from EDAX measurements were 0.3%, 1.5%, and 2.6%, respectively. The content of Mn in Cu_2O is within the limit of highest concentration of 3% in the formation of single phase.[30]

Figure 3 shows the XPS results of the samples CP3 and HMnCP3. Figure 3(a) gives the XPS spectra of the core levels of Cu $2p_{3/2}$ and Cu $2p_{1/2}$ for the undoped nanoparticles CP3 to be approximately 932.59 and 952.86 eV, which are in excellent agreement with the values of Cu^+ in pure Cu_2O.[16] Cu $2p_{3/2}$ peak of Cu^+ at 932.59 eV was accompanied by a series of satellites (peaks 2 and 3) on the high-binding-energy side, which is the evident of an open $3d^9$ shell, corresponding to the Cu^{2+} state.[16,31,32] The XRD spectra of the Cu_2O nanoparticles do not show any evidence of CuO phase, but XPS indicates the presence of Cu^{2+} ions in the nanoparticles samples, suggests that CuO is present only on the surface of the Cu_2O nanoparticles in the form of amorphous shell.[17] This CuO may result from the oxidation of Cu_2O on the surface. The highest doped sample HMnCP3 shown in the Fig. 3(a) also gives the similar XPS spectrum of the core

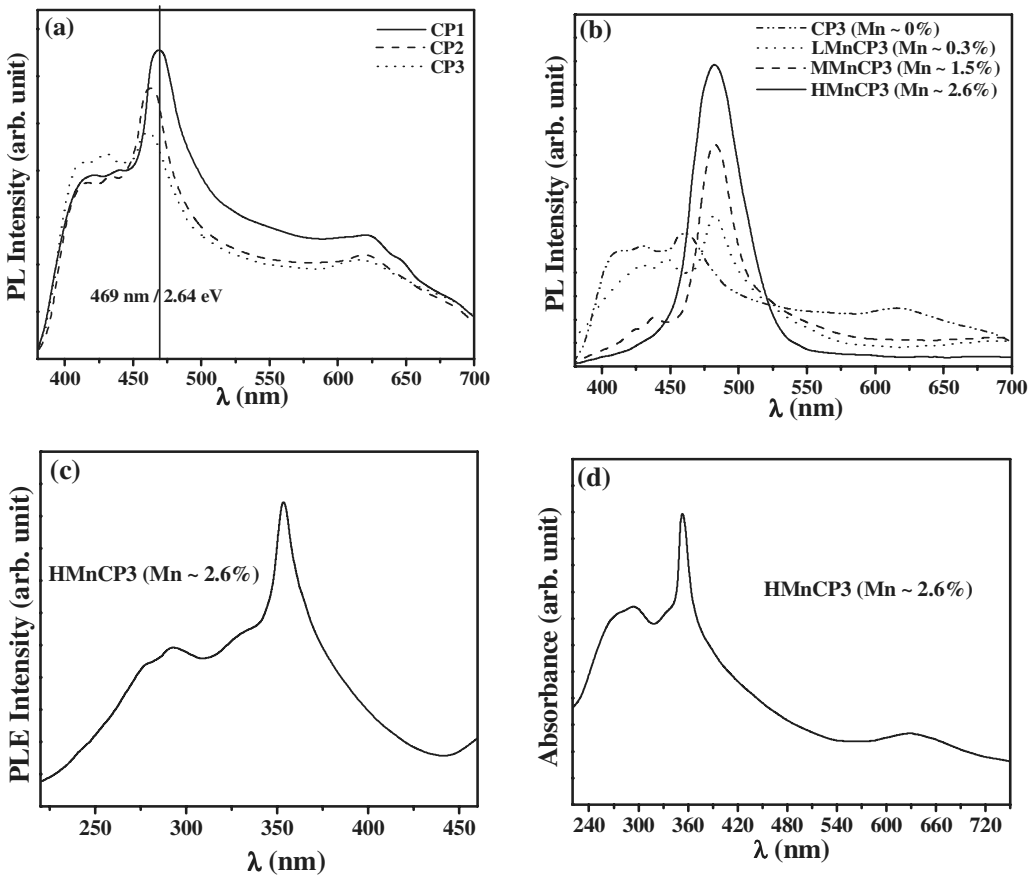

FIG. 4. [(a) and (b)] Photoluminescence spectra of all the undoped and doped Cu_2O samples, respectively. (c) PLE and (d) UV-visible absorption spectra of the highest doped sample HMnCP3.

levels of Cu $2p_{3/2}$ and Cu $2p_{1/2}$. The shift to the lower energy side of the Cu $2p$ peak occurs in the doped sample, which is good agreement to the observations by Gao *et al.*[30] Figure 3(b) shows the Mn $2p$ core level spectrum of highest Mn doped sample HMnCP3. Two broad peaks corresponding to the Mn $2p_{3/2}$ and Mn $2p_{1/2}$ are approximately at 641.18 and 653.11 eV, attributed to Mn^{2+}.[33] Thus it may be concluded that the Mn was doped in the Cu_2O nanoparticles in the form of Mn^{2+}.

To study the variations of the photophysical properties of the nanoparticles with size and doping concentration, the steady-state PL and PL decays of the all undoped and doped samples were measured at room temperature. Figure 4(a) shows the PL spectra of the nanoparticles CP1, CP2, and CP3 recorded with excitation wavelength 340 nm. One violet and two blue emission peaks around 421 nm (2.94 eV), 440 nm (2.81 eV), and 469 nm (2.64 eV) are found for the sample CP1 having crystallite diameter ~16 nm. These emissions are expected due to the excitonic transitions from the different sub levels of the CB to the Cu *d*-shells of the VBs,[8,34] which will be discussed later using schematic band diagram. All the peaks were blue shifted with decreasing the size of the nanoparticles, indicating the quantum confinement effect of the excitonic transition expected for Cu_2O nanoparticles.[17] It was found from the literature that the quantum confinement threshold of Cu_2O nanocrystals was 14 nm.[13] Thus the quantum confinement effect was observed for the samples CP2 and CP3 having sizes ~8–11 nm. The well-known series of yellow excitonic emissions of the Cu_2O are also observed between 600 and 700 nm for all the nanoparticles. Figure 4(b) shows the room temperature PL spectra of the all doped samples. The emission peaks of the undoped sample CP3 were red shifted in the doped samples. This phenomenon has been explained as mainly due to *pd-d* exchange interactions between the band electrons of Cu_2O and the localized *d* electrons of the Mn^{2+} ions substituting metal ions Cu^+. The *p-d* and *d-d* exchange interactions give rise to a lowering of CB energy and upward shifting of VB edge leading to lowering the emission energies.[35,36] Moreover the intensities of the emissions around 428 and 447 nm for the lowest doped sample LMnCP3 were decreased with increasing Mn concentration and ultimately quenched in the highest doped sample HMnCP3. The emission around 482 nm (2.57 eV) becomes more pronounced with doping. The incorporation of Mn in the Cu_2O lattice gives splitted Mn *d* bands. The emission around 2.57 eV may be due to the transition $^4T_2 \rightarrow {}^6A_1$ of Mn^{2+} ions in analogy to the case of MnO.[37,38] Figure 4(c) shows the photoluminsecence excitation (PLE) spectrum of the highest doped sample HMnCP3 recorded by fixing the emission at 482 nm, which gives the maximum PLE intensity at the energy 3.51 eV (353 nm). The PLE result collected by monitoring the Mn^{2+} $^4T_2 \rightarrow {}^6A_1$ transition also indicate, that energy transfer from the photoexcited Cu_2O nanocrystals to the Mn^{2+} gives rise to the blue emission.[20,39] The UV-visible absorption spectrum of sample HMnCP3 shown in the Fig. 4(d), gives a weak broad peak at

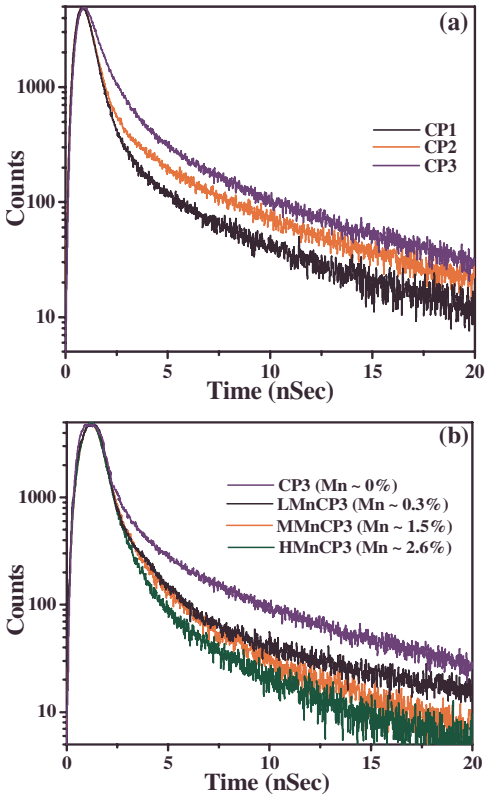

FIG. 5. (Color online) Photoluminescence decays of all the (a) undoped and (b) doped Cu_2O samples.

632 nm (1.96 eV) along with four absorption bands at about 280, 293, 334, and 352 nm. The four peaks at higher energy side may be due to the absorptions of Cu_2O nanocrystals whereas the peak at the lower energy may be attributed to the band gap transition of CuO, present at the surface of the Cu_2O nanocrystals, supported by the XPS studies.[16] If Mn^{2+} is incorporated in the CuO rather than Cu_2O, then the emission related to the Mn^{2+} $^4T_2 \rightarrow {}^6A_1$ transition is not possible to observe, since the energy band of CuO associated to the absorption of 1.96 eV lies below the Mn $^4T_2$ level.[40] Thus from the optical and XPS studies, it may be concluded that the Cu^+ ion is substituted by the Mn^{2+} ion in the Cu_2O lattice.

To explain the effects of the particle size and doping on the relaxations between the different energy states of the Cu_2O nanoparticles, the life times of the all undoped and doped samples were measured by utilizing the TCSPC. Figure 5(a) shows the PL decays of the undoped samples CP1–CP3. The fluorescence decays of all the nanoparticles have triexponential ($n=3$) functions as defined in Eq. (1). The values of goodness of fit parameter, χ^2 near unity as shown in Table II indicate a good fit to experimental data. The best fitted parameters α_i and τ_i are shown in Table II. The estimated life times vary from nanoseconds to picoseconds. The average decay time $\langle\tau\rangle$ calculated using Eq. (2) increases continuously with decreasing size of the nanoparticles as shown in Table II. Figure 5(b) shows the PL decays of the doped samples. From Table II it is noted that the average life times of the Cu_2O nanoparticles decreases continuously with increasing doping concentration.

The decay dynamics and the sources of the different PL emissions of the nanoparticles can be understood from the electronic energy band structure of Cu_2O. Recently, Önsten *et al.*[41] showed that the VB structure of Cu_2O has Cu 3*d*, hybridized Cu 3*d*-4*s* and O 2*p* character from angle resolved photoelectron spectroscopy. The CB are derived from hybridized Cu 3*d*-4*s* and O 2*p* states.[42,43] Band structure calculations based on local density approximation including on site Coulomb and self interaction corrections indicate that the VB and CB structures are consistent with experiments. Figure 6(a) shows the schematic diagram of angular momentum decomposed energy bands of the bulk Cu_2O. Transitions from the top of VB to the bottom of CB ($3d \rightarrow 4s$) are forbidden according to selection rules. Theoretically it was predicted that transition probabilities from many bands below the top of VB to CB are negligible.[44,45] Valence Cu 3*d* band width is about 2 eV and CBs 3*d*-4*s* are almost 2.17 eV above VB. 340 nm (3.65 eV) pulses may excite electrons from the Cu 3*d* band of VB to O 2*p* of CB since the transitions from Cu 3*d* of VB $\rightarrow$ Cu 3*d*-4*s* of CB and Cu 3*d*-4*s* of VB $\rightarrow$ Cu 3*d*-4*s* of CB are parity forbidden. Quantum confinement of electrons in the nanoparticles gives rise to the splitting of energy levels with respect to bulk.[8,46,47] Thus the relaxations of the electrons occur from the different subenergy levels of O 2*p* band to Cu 3*d* band, which give rise one violet and two blue emissions. (Fig. 6) The slowest component τ_2 may be due to the violet emission and other two components τ_1 and τ_3 may be due to the two blue emissions. The fractional contribution ($\%f_3$) of the fast component τ_3 decreases and the contributions ($\%f_2$ and $\%f_1$) of the slow components τ_2 and τ_1 increase with decreasing particle size (Table II), indicates that the splitting of the energy bands due to the quantum confinement is more prominent with decreasing particle size. Moreover it is well known that the electronic states are

TABLE II. Best fitted parameters of multiexponential components defined in Eqs. (1)–(3).

Sample name	Pre-exponential functions			Decay life times (ns)				Fractional contribution			Goodness of fit parameter
	α_1	α_2	α_3	τ_1	τ_2	τ_3	$\langle\tau\rangle$	f_1	f_2	f_3	(χ^2)
CP1	0.000 73	0.000 19	0.915	1.993	8.16	0.0148	0.97	0.10	0.09	0.81	1.16
CP2	0.001 36	0.000 35	0.998	2.519	9.67	0.0184	1.68	0.14	0.13	0.73	1.11
CP3	0.012 90	0.0021	0.985	1.44	7.71	0.0358	2.18	0.27	0.23	0.50	1.10
LMnCP3	0.009 00	0.0006	0.990	1.56	7.24	0.0260	1.22	0.31	0.11	0.58	1.09
MMnCP3	0.000 89	0.000 21	0.994	2.40	7.28	0.0201	0.71	0.09	0.06	0.85	1.01
HMnCP3	0.000 28	0.000 05	0.999	3.16	8.59	0.0187	0.34	0.04	0.02	0.94	1.07

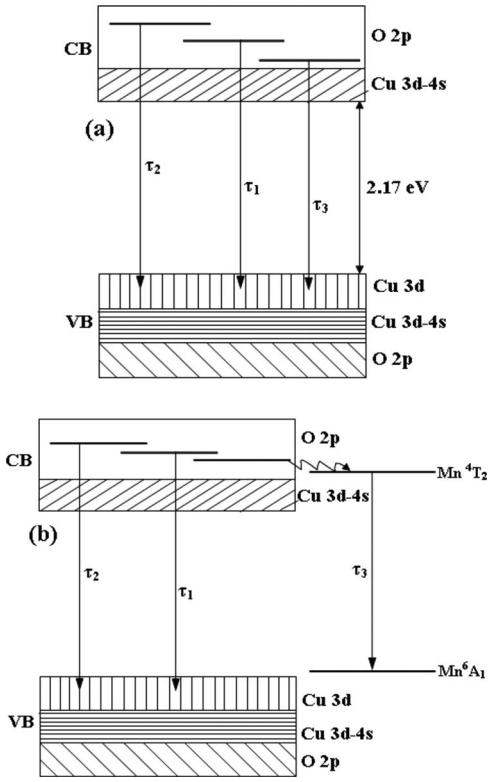

FIG. 6. Schematic diagrams of angular momentum decomposed energy bands of the bulk (a) undoped Cu_2O and (b) Mn doped Cu_2O.

localized due to the confinement effect, therefore it reduces the oscillator strength and as a result the life times of the nanoparticles increase with decreasing the size.[48] Divalent Mn has d^5 electronic configuration. In octahedral crystal field, d states are split into $^6A_1$ and $^4T_2$ levels. Supercell calculations predict that Mn d states are formed within VB and CB regions of undoped Cu_2O.[49] A representative band diagram of Cu_2O doped with Mn is shown in Fig. 6(b). The maximum portion of the photogenerated electrons in the O $2p$ level may relax nonradiatively to the Mn $^4T_2$ level and then relax radiatively to the Mn $^6A_1$ level lying near VB of Cu_2O. These successive transitions give rise to prominent emission peak near 2.57 eV. Thus the contribution ($\%f_3$) of the fast component of decay τ_3 related to the emission around 2.57 eV increases compared to the contributions ($\%f_2$ and $\%f_1$) of other two τ_2 and τ_1 with doping (Table II) and ultimately the quenching of the two slow components occurs with Mn doping concentration of 2.6% of the sample HMnCP3. It is considered that the shortened decay time of the Mn doped Cu_2O nanoparticles originates from the effective energy transfer process from O $2p$ to Mn $3d$ levels.[18] Moreover the quenching of these two emissions of the Cu_2O nanoparticles may occur due to the strain induced defects increasing with doping.[50] Thus it may be concluded that small percentage of Mn doping might quenched the multiple emissions of the Cu_2O nanoparticles and only blue light emits from the nanoparticles.

IV. CONCLUSIONS

The Cu_2O nanoparticles having crystallite diameters ~8–16 nm were obtained by a simple solvothermal method using dextrose as the reducing agent. The effects of the variations of size and Mn doping on the photophysical properties of the nanoparticles were studied. The XPS studies clearly showed that the Mn was incorporated into the Cu_2O lattice as Mn^{2+}. The Luminescence studies revealed the quantum confinement effect in the nanoparticles. The incorporation of the Mn in the Cu_2O nanoparticles having average crystallite diameter ~8 nm quenched the multiple emissions of the Cu_2O nanoparticles and favored only blue light emitted from the nanoparticles. Thus it may be concluded that the introduction of the small percentage of Mn may tune the emission of the Cu_2O nanoparticles.

[1] C. A. N. Fernando, L. A. A. De Silva, R. M. Mehra, and K. Takahashi, Semicond. Sci. Technol. **16**, 433 (2001).
[2] G. K. Paul, R. Ghosh, S. K. Bera, S. Bandyopadhyay, T. Sakurai, and K. Akimoto, Chem. Phys. Lett. **463**, 117 (2008).
[3] C. M. McShane and K.-S. Choi, J. Am. Chem. Soc. **131**, 2561 (2009).
[4] J. Li, L. Liu, Y. Yu, Y. Tang, H. Li, and F. Du, Electrochem. Commun. **6**, 940 (2004).
[5] L. Xu, L.-P. Jiang, and J.-J. Zhu, Nanotechnology **20**, 045605 (2009).
[6] J. Antony, Y. Qiang, M. Faheem, D. Meyer, D. E. McCready, and M. H. Engelhard, Appl. Phys. Lett. **90**, 013106 (2007).
[7] *CRC Handbook of Chemistry and Physics*, 74th ed. (CRC, Boca Raton, 1993), pp. 4–147.
[8] G. P. Pollack and D. Trivich, J. Appl. Phys. **46**, 163 (1975).
[9] V. T. Agekyan, Phys. Status Solidi A **43**, 11 (1977).
[10] R. J. Elliott, Phys. Rev. **124**, 340 (1961).
[11] N. Caswell and P. Y. Yu, Phys. Rev. B **25**, 5519 (1982).
[12] S. Deki, K. Akamatsu, T. Yano, M. Mizuhata, and A. Kajinami, J. Mater. Chem. **8**, 1865 (1998).
[13] Y. Chang, J. J. Teo, and H. C. Zeng, Langmuir **21**, 1074 (2005).
[14] Z. Yang, C.-K. Chiang, and H.-T. Chang, Nanotechnology **19**, 025604 (2008).
[15] B. Balamurugan, I. Aruna, and B. R. Mehta, Phys. Rev. B **69**, 165419 (2004).
[16] M. Yin, C.-K. Wu, Y. Lou, C. Burda, J. T. Koberstein, Y. Zhu, and S. O'Brien, J. Am. Chem. Soc. **127**, 9506 (2005).
[17] K. Borgohain, N. Murase, and S. Mahamunia, J. Appl. Phys. **92**, 1292 (2002).
[18] D. Kim, M. Miyamoto, and M. Nakayama, J. Appl. Phys. **100**, 094313 (2006).
[19] Y. S. Wang, J. P. Thomas, and P. O'Brien, J. Phys. Chem. B **110**, 21412 (2006).
[20] T. J. Norman, Jr., D. Magana, T. Wilson, C. Burns, and J. Z. Zhang, J. Phys. Chem. B **107**, 6309 (2003).
[21] M. Wei, N. Braddon, D. Zhi, P. A. Midgley, S. K. Chen, M. G. Blamire, and J. L. MacManus-Driscoll, Appl. Phys. Lett. **86**, 072514 (2005).
[22] L. Pan, H. Zhu, C. Fan, W. Wang, Y. Zhang, and J. Q. Xiao, J. Appl. Phys. **97**, 10D318 (2005).
[23] M. Ivill, M. E. Overberg, C. R. Abernathy, D. P. Norton, A. F. Hebard, N. Theodoropoulou, and J. D. Budai, Solid-State Electron. **47**, 2215 (2003).
[24] JCPDS Card No. 05–0667.
[25] P. Kameli, H. Salamati, and A. Aezami, J. Appl. Phys. **100**, 053914 (2006).
[26] K. Venkateswara Rao and C. S. Sunandana, Solid State Commun. **148**, 32 (2008).
[27] E. Wu, J. Appl. Crystallogr. **22**, 506 (1989).
[28] R. D. Shannon, Acta Crystallogr., Sect. A: Cryst. Phys., Diffr., Theor. Gen. Crystallogr. **32**, 751 (1976).
[29] K. Das, S. K. Panda, and S. Chaudhuri, Appl. Surf. Sci. **253**, 5166 (2007).
[30] K. H. Gao, Z. Q. Li, T. Du, E. Y. Jiang, and Y. X. Li, Phys. Rev. B **75**, 174444 (2007).
[31] Y. Yu, L.-L. Ma, W.-Y. Huang, J.-L. Li, P.-K. Wong, and J. C. Yu, J. Solid State Chem. **178**, 1488 (2005).
[32] J. Ghijsen, L. H. Tjeng, J. v. Elp, H. Eskes, J. Westerink, and G. A. Sawatzky, Phys. Rev. B **38**, 11322 (1988).
[33] Y.-F. Han, F. Chen, Z. Zhong, K. Ramesh, L. Chen, and E. Widjaja, J. Phys. Chem. B **110**, 24450 (2006).
[34] J. P. Dahl and A. C. Switendick, J. Phys. Chem. Solids **27**, 931 (1966).
[35] Y. R. Lee, A. K. Ramdas, and R. L. Agarwal, Phys. Rev. B **38**, 10600

(1988).
[36]Y. D. Kim, S. L. Cooper, M. V. Klein, and B. T. Jonker, Phys. Rev. B **49**, 1732 (1994).
[37]R. Viswanatha, S. Sapra, S. Sen Gupta, B. Satpati, P. V. Satyam, B. N. Dev, and D. D. Sarma, J. Phys. Chem. B **108**, 6303 (2004).
[38]C. E. Deshprandhe and S. K. Date, J. Mater. Sci. Lett. **3**, 563 (1984).
[39]D. J. Norris, N. Yao, F. T. Charnock, and T. A. Kennedy, Nano Lett. **1**, 3 (2001).
[40]R. Beaulac, P. I. Archer, X. Liu, S. Lee, G. M. Salley, M. Dobrowolska, J. K. Furdyna, and D. R. Gamelin, Nano Lett. **8**, 1197 (2008).
[41]A. Önsten, M. Månsson, T. Claesson, T. Muro, T. Matsushita, T. Nakamura, T. Kinoshita, U. O. Karlsson, and O. Tjernberg, Phys. Rev. B **76**, 115127 (2007).
[42]A. Filippetti and V. Fiorentini, Phys. Rev. B **72**, 035128 (2005).
[43]R. Laskowski, P. Blaha, and K. Schwarz, Phys. Rev. B **67**, 075102 (2003).
[44]X. Nie, S.-H. Wei, and S. B. Zhang, Phys. Rev. B **65**, 075111 (2002).
[45]W. Y. Ching, Y.-N. Xu, and K. W. Wong, Phys. Rev. B **40**, 7684 (1989).
[46]S. Jana and P. K. Biswas, Mater. Lett. **32**, 263 (1997).
[47]R. Rossetti, J. L. Ellison, J. M. Gibson, and L. E. Brus, J. Chem. Phys. **80**, 4464 (1984).
[48]H. Wang, C. de Mello Donegá, A. Meijerink, and M. Glasbeek, J. Phys. Chem. B **110**, 733 (2006).
[49]M. Sieberer, J. Redinger, and P. Mohn, Phys. Rev. B **75**, 035203 (2007).
[50]X. D. Pi, R. Gresback, R. W. Liptak, S. A. Campbell, and U. Kortshagen, Appl. Phys. Lett. **92**, 123102 (2008).